

Journal of Turbomachinery Journal

Copy of e-mail Notification

Journal of Turbomachinery Published by ASME

Dear Author,

Congratulations on having your paper accepted for publication in the ASME Journal Program.

Your page proof is available in PDF format from the ASME Proof Download & Corrections site here:

<http://115.111.50.156/jw/AuthorProofLogin.aspx?pwd=06f0897d6af0>

Login: your e-mail address

Password: 06f0897d6af0

Please keep this email in case you need to refer back to it in the future.

You will need Adobe Acrobat Reader software to view the file. This is free software and a download link is provided when you log in to view your proofs.

Responsibility of detecting errors rests with the author. Please review the page proofs carefully and:

- 1) Answer any queries on the first page "Author Query Form"
- 2) Proofread any tables and equations carefully
- 3) Check to see that any special characters have translated correctly

RETURNING CORRECTIONS:

To return corrections, please use the ASME Proof Download & Corrections Submission Site (link above) and provide either:

1. Annotated PDF
2. Text entry of corrections, with line numbers, in the text box provided

Additional files, as necessary, can also be uploaded through the site.

SPECIAL NOTES:

Your Login and Password are valid for a limited time. Please reply within 48 hours. Your prompt attention to and return of page proofs will speed the publication of your work.

For all correspondence, please include your article no. (TURBO-12-1212) in the subject line.

This e-proof is to be used only for the purpose of returning corrections to the publisher.

If you have any questions, please contact: asme.cenveo@cenveo.com.

Sincerely,

Mary O'Brien, Journal Production Manager

STATEMENT OF EDITORIAL POLICY AND PRACTICE

The Technical Committee on Publications and Communications (TCPC) of ASME aims to maintain a high degree of technical, literary, and typographical excellence in its publications. Primary consideration in conducting the publications is therefore given to the interests of the reader and to safeguarding the prestige of the Society.

To this end the TCPC confidently expects that sponsor groups will subject every paper recommended by them for publication to careful and critical review for the purpose of eliminating and correcting errors and suggesting ways in which the paper may be improved as to clarity and conciseness of expression, accuracy of statement, and omission of unnecessary and irrelevant material. The primary responsibility for the technical quality of the papers rests with the sponsor groups.

In approving a paper for publication, however, the TCPC reserves the right to submit it for further review to competent critics of its own choosing if it feels that this additional precaution is desirable. The TCPC also reserves the right to request revision or condensation of a paper by the author or by the staff for approval by the author. It reserves the right, and charges the editorial staff, to eliminate or modify statements in the paper that appear to be not in good taste and hence likely to offend readers (such as obvious advertising of commercial ventures and products, comments on the intentions, character, or acts of persons and organizations that may be construed as offensive or libelous), and to suggest to authors rephrasing of sentences where this will be in the interest of clarity. Such rephrasing is kept to a minimum.

Inasmuch as specific criteria for the judging of individual cases cannot, in the opinion of the TCPC, be set up in any but the most general rules, the TCPC relies upon the editorial staff to exercise its judgment in making changes in manuscripts, in rearranging and condensing papers, and in making suggestions to authors. The TCPC realizes that the opinions of author and editor may sometimes differ, and hence it is an invariable practice that no paper is published until it has been passed on by the author. For this purpose page proofs of the edited paper are sent to the author prior to publication in a journal. Changes in content and form made in the proofs by authors are followed by the editor except in cases in which the Society's standard spelling and abbreviation forms are affected.

If important differences of opinion arise between author and editor, the points at issue are discussed in correspondence or interview, and if a solution satisfactory to both author and editor is not reached, the matter is laid before the TCPC for adjustment.

AUTHOR QUERY FORM

 ASME <small>SETTING THE STANDARD</small>	<p>Journal: J. Turbomach.</p> <p>Article Number: TURBO-12-1212</p>	<p>Please provide your responses and any corrections by annotating this PDF and uploading it to ASME's eProof website as detailed in the Welcome email.</p>
--	--	---

Dear Author,

Below are the queries associated with your article; please answer all of these queries before sending the proof back to Cenveo. Production and publication of your paper will continue after you return corrections or respond that there are no additional corrections.

Location in article	Query / Remark: click on the Q link to navigate to the appropriate spot in the proof. There, insert your comments as a PDF annotation.
AQ1	Please spell out the acronym "MAV" in the sentence beginning "Pereira performed an experimental study..."
AQ2	As per ASME style, each reference must have its own number. Ref. 2 has been renumbered as Refs. 2 and 3. Please provide a separate page range for each reference.
AQ3	Please provide a page range for Ref. 3.
AQ4	Please provide a page range for Ref. 4.
AQ5	Please provide a complete list of authors, volume number, and page range for Ref. 21.
AQ6	Please provide a complete list of authors for Ref. 22.

Thank you for your assistance.

Author Proof

Tip Clearance Investigation of a Ducted Fan Used in VTOL Unmanned Aerial Vehicles—Part 1: Baseline Experiments and Computational Validation

1 **Ali Akturk¹**

2 e-mail: akturkali@gmail.com

3 **Cengiz Camci²**

4 Professor

5 e-mail: cxc11@psu.edu

6 Turbomachinery Aero-Heat Transfer Laboratory,
7 Department of Aerospace Engineering,
8 Pennsylvania State University,
9 University Park, PA 16802

Ducted fans that are popular choices in vertical take-off and landing (VTOL) unmanned aerial vehicles (UAV) offer a higher static thrust/power ratio for a given diameter than open propellers. Although ducted fans provide high performance in many VTOL applications, there are still unresolved problems associated with these systems. Fan rotor tip leakage flow is a significant source of aerodynamic loss for ducted fan VTOL UAVs and adversely affects the general aerodynamic performance of these vehicles. The present study utilized experimental and computational techniques in a 22 in. diameter ducted fan test system that has been custom designed and manufactured. The experimental investigation consisted of total pressure measurements using Kiel total pressure probes and real time six-component force and torque measurements. The computational technique used in this study included a 3D Reynolds-averaged Navier Stokes (RANS) based computational fluid dynamics model of the ducted fan test system. Reynolds-averaged Navier-Stokes simulations of the flow around the rotor blades and duct geometry in the rotating frame of reference provided a comprehensive description of the tip leakage and passage flow. The experimental and computational analysis performed for various tip clearances were utilized in understanding the effect of the tip leakage flow on the aerodynamic performance of ducted fans used in VTOL UAVs. The aerodynamic measurements and results of the RANS simulations showed good agreement, especially near the tip region. [DOI: 10.1115/1.4023468]

7 1 Introduction

8 The flow field resulting from the region between the stationary
9 duct and rotor tip of a ducted fan is complicated because of the
10 interaction of the tip leakage flow, annulus wall boundary layer,
11 and rotor wake. The inherent pressure difference between the
12 pressure side and suction side of the blade tip generates a tip
13 leakage flow. The leakage flow also rolls into a highly three
14 dimensional tip leakage vortex with significantly turbulent and
15 unsteady flow features in each passage. The tip leakage vortex is
16 a complex flow phenomenon that is one of the dominant mechanisms
17 of noise generation by unsteady interactions in a turbomachinery
18 system. It is a significant energy loss mechanism in the
19 ducted fans.

20 This paper describes investigations on the tip clearance flow for
21 ducted fans. The common design principle of a ducted fan is to
22 ensure that the tip clearance is as small as possible to reduce tip
23 leakage losses and improve the aerodynamic performance. Indeed,
24 this is still the case for ducted fans used in VTOL UAVs; the
25 clearance is unavoidably kept large because of the operating
26 conditions. There are many small diameter VTOL UAV systems
27 using internal combustion (IC) engines as the power source. The
28 IC engine driven systems suffer from strong mechanical
29 vibrations.

30 There have been a limited number of studies about the three
31 dimensional flow structure of leakage vortex in axial flow fans

and compressors in the literature [1–6]. Inoue and Kuroumaru et al. [7] made detailed flow measurements before and behind an axial flow rotor with different tip clearances. In their study, they investigated the clearance effect on the behavior of tip leakage flow. Furukawa and Inoue et al. [8] also investigated the breakdown of the tip leakage vortex in a low speed axial flow compressor. Reducing the tip leakage mass flow rate, in general, improves the aerodynamic performance of axial flow fans and compressors. Implementation of treatments in the nonrotating part over the blade tip is also an efficient method for tip leakage flow reduction. References [9,10] investigate different casing treatments for axial flow compressors.

32 The wake developed from an axial flow fan has a strong
33 influence on the system performance. It is a significant source of
34 aerodynamic loss and affects the efficiency and vibration charac-
35 teristics. References [11–13] deal with extensive investigations of
36 the wake flow features such as the mean velocities, turbulence,
37 and decay characteristics on turbomachinery performance. The
38 wake flow system is likely to interact with the complex flow sys-
39 tem originating in the tip gap region.

40 Few authors have investigated the influence of large tip clear-
41 ances in turbomachinery components. Large tip clearances are not
42 typically found within axial flow fans and compressors designed
43 for aero-engines. Williams et al. [14] investigated large tip clear-
44 ances in the high pressure compressor stages used in industrial gas
45 turbines. They have carried out a comprehensive study on two dif-
46 ferent compressor cascades. They used five-hole pressure probe
47 measurements upstream and downstream of the cascades. The
48 authors have shown that tip leakage flow is a more important
49 parameter influencing the rotor exit flow pattern than blade shape.

50 Ducted fan VTOL UAVs need to fly in a broad range of atmos-
51 pheric conditions because of their complicated missions. Their
52

¹Currently working at Siemens Energy Inc.

²Corresponding author.

Contributed by the International Gas Turbine Institute (IGTI) of ASME for publication in the JOURNAL OF TURBOMACHINERY. Manuscript received November 5, 2012; final manuscript received December 8, 2012; published online xx xx, xxxx. Assoc. Editor: David Wisler.

PROOF COPY [TURBO-12-1212]

AQ1

64 performance is highly affected by large tip clearance. There have
 65 been only a few studies about ducted fan aerodynamic and aero-
 66 mechanical performance. Pereira performed an experimental
 67 study on the effects of various shroud profile shapes on the per-
 68 formance of MAV-scale shrouded rotors [15]. Seventeen ducted
 69 fan models with a nominal rotor diameter of 16 cm (6.3 in.) and
 70 various values of diffuser expansion angle, diffuser length, inlet
 71 lip radius, and blade tip clearance were tested at various rotor col-
 72 lective angles. Tests performed for an open rotor and a single
 73 shrouded-rotor model at a single collective in translational flight,
 74 at angles of attack from 0 deg (axial flow) to 90 deg (edgewise
 75 flow) and at various advance ratios, are reported.

76 Martin and Tung [16] tested a ducted fan V/STOL UAV with a
 77 10-inch diameter rotor. They measured aerodynamic loads on the
 78 vehicle for different angles of attack (from 0 deg to 110 deg) in
 79 hover and different crosswind velocities. Both models were tested
 80 with fixed-pitch propellers of varying diameters, in order to test
 81 tip clearances from 1% to 4% (based on the rotor tip radius). They
 82 also included hot-wire velocity surveys at the inner and outer
 83 surfaces of the duct and across the downstream wake, emphasizing
 84 the effect of the tip gap on the produced thrust force. In addition,
 85 their study showed the effect of the leading edge radius of
 86 the duct on the stall performance and stability of the vehicle. They
 87 have shown that the thrust of the system decreases with an
 88 increasing tip gap height. Their results also showed that for lower
 89 rotational speeds, the open rotor thrust was higher than the ducted
 90 fan thrust. They explained this by pointing out the increase in vis-
 91 cous losses inside the duct for low rotational speed operations.

92 Martin and Boxwell [17] tested two ducted fan models that
 93 were designed to effectively eliminate the tip leakage. Both
 94 models were derived from the baseline (10-inch inner-diameter
 95 shroud), which is explained in their previous study [16]. In their
 96 first design, they created a notch and fit the propeller inside the

97 notch. In their second design, a rearward-facing step was cut into
 98 the inner shroud. The computational analysis resulted in an
 99 increase in the inlet lip suction and an increase in performance.
 100 However, the experimental thrust and power measurements
 101 showed no difference in the performance of these designs when
 102 compared to their baseline duct.

103 In the present investigation, experimental and computational
 104 methods were used to investigate the effect of tip clearance flow
 105 on ducted fan aerodynamic performance. A 22 in. ducted fan
 106 test system was designed and manufactured for experimental
 107 investigations. Total pressure measurements were performed at
 108 the downstream of the fan rotor using a traversing Kiel probe. The
 109 inlet total pressure and axial velocity were also monitored at the
 110 midspan location. The aeromechanical performance of the ducted
 111 fan was measured using a six axis force and moment transducer.
 112 Besides the experimental measurements, computational analyses
 113 were carried out for the ducted fan system in the hover condition.
 114 The main goal of this paper is to investigate the large tip clearance
 115 effect in ducted fans for VTOL UAV applications. The experi-
 116 mental data obtained were also used to validate the computational
 117 method outlined in this paper. The computational method is also
 118 going to be used in the development of tip treatments. The results
 119 from an investigation dealing with the new tip treatments
 120 designed and analyzed using this validated computational
 121 approach are presented in an accompanying paper by Akturk and
 122 Camci [18].

2 Experimental Method

123 **2.1 Facility Description.** The 22 in. diameter ducted fan test
 124 system with a realistic disk loading found in most present day
 125 VTOL UAV systems is shown in Fig. 1. The main components in
 126 the flow path of this facility are listed as follows:

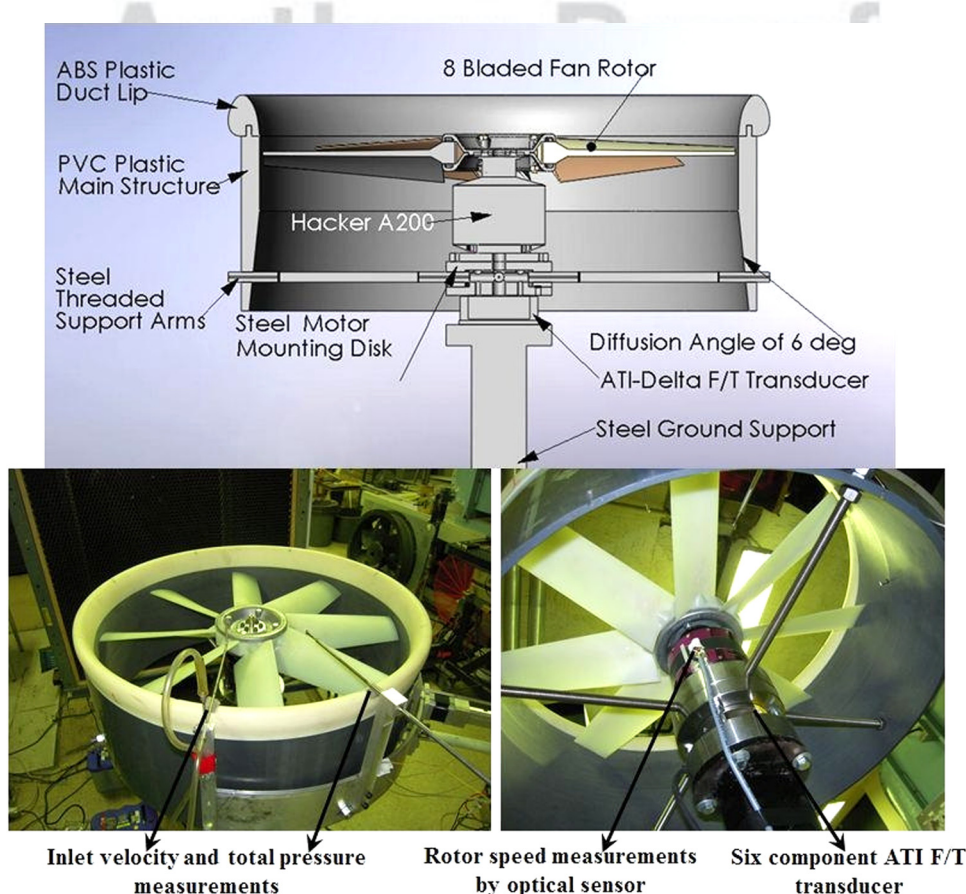


Fig. 1 Schematic and instrumentation of the 22 in. diameter ducted fan system

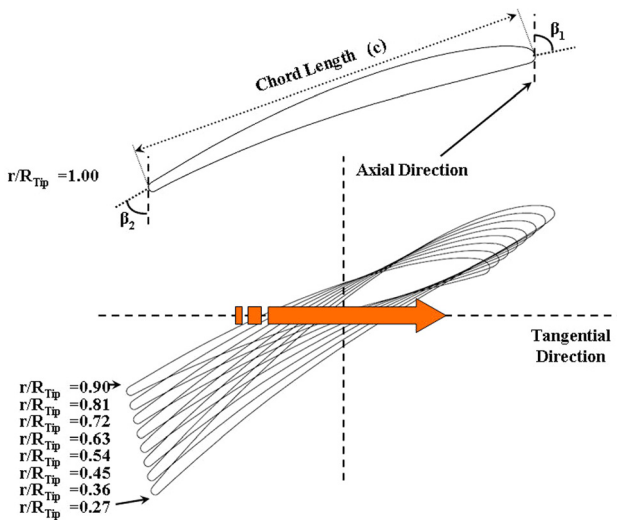


Fig. 2 Blade profiles at various radial stations

- inlet lip section (replaceable)
- eight-bladed axial fan rotor
- 20 hp DC brushless electric motor
- diffuser section
- six component force and torque measurement system

Figure 1 shows the main components of the instrumentation integrated into this research facility. The test system is equipped with a radially traversing Kiel total pressure probe downstream of the axial flow fan rotor, a stationary total pressure probe at the inlet of the duct, an optical once-per-rev sensor, a Pitot probe for velocity measurements at the duct inlet, and an ATI six component force and torque measurement transducer. The system also has a number of thermocouples and various electrical monitoring systems for electrical safety.

2.2 Ducted Fan Model. The ducted fan used in the current experiments is composed of a shroud, axial flow fan, inlet lip, and exit diffuser. The shroud is manufactured from thermoplastic material and has an inner radius of 11.15 in. It is connected to the main support using four 12.7 mm (0.5 in.) diameter stainless steel threaded circular rods. Threaded rods connect the shroud to the central support system. The center support holds the ducted fan so that the fan rotor is about three rotor diameters away from the ground, which guarantees that the measurements are free from the ground effect.

The 22 in. diameter ducted fan was designed to provide a realistic disk loading typical of VTOL UAVs. The 22 in. diameter

ducted fan shown in Fig. 1 provides 828.3 Pa (17.31b/ft²) disk loading under nominal operating conditions (3500 rpm).

The geometry of the duct inlet lip shape can be described by two distinct characteristics: the wall thickness (t_w) and the leading edge radius of curvature (ρ_{LE}). Wall thickness is the maximum thickness of the airfoil shape used to make up the wall of the duct and the leading edge radius of curvature describes the roundness of the duct lip. The inlet lip shape was designed to have a relatively small leading edge radius. The reduced leading edge radius usually allows the adverse pressure gradient to gradually change inside the lip. The changing pressure gradient gradually helps reduce inlet lip separations inside the duct lip, especially under edgewise flight conditions. The t_w and ρ_{LE} used for this ducted fan were 11% and 3.61% of the duct chord, respectively. The diffuser section was designed to augment the thrust generated by the ducted fan. The diffuser half angle at the exit is 6 deg. The axial length of the diffuser is about 117.85 mm (4.64 in.).

2.2.1 Fan Rotor. The eight-bladed fan rotor was designed and manufactured by Multi-Wing International. The fan blades were designed for a high flow coefficient. The rotor blades were manufactured from a high quality thermoplastic (glass reinforced polyamide). The rotor blades are attached to a custom designed aluminum hub. This specific hub system allows for a quick replacement of the rotor assembly in this research facility. Figure 2 shows the blade profiles at various radial stations. Table 1 presents the fan rotor and blade section geometrical properties.

A 20 hp A200-6 brushless electric motor (Hacker) directly drives the axial flow fan rotor in the 22 in. diameter ducted fan research facility. The electric motor was controlled by an electronic speed controller (MasterSPIN-220-OPTO ESC). Electrical power for the motor was supplied by four deep cycle lead acid batteries connected in series. Due to the high torque characteristic of the electric motor, the electric current and temperature of the motor was continuously monitored for operational safety.

2.3 Instrumentation of the 22 Inch Ducted Fan

2.3.1 Rotor Exit Total Pressure Measurements. Fan rotor exit total pressure measurements were performed by using a Kiel total pressure probe. The Kiel total pressure probe, having a 5 mm diameter total head, was traversed in the radial direction using a precision linear traverse mechanism. The total pressure probe was always located 45.72 mm downstream of the fan rotor exit plane at 50% blade span (mid-span).

The Kiel probe, manufactured by United Sensors Corporation, is relatively insensitive to the incoming angle of the flow (yaw angle). The range of insensitivity to misalignment for this probe is about ± 52 deg to see a more than 1% deviation from the inlet dynamic head [19]. The accurate orientation of the Kiel probe in a

Table 1 Fan rotor geometric and blade section properties

Rotor hub radius	Blade section properties			
	r/R_{tip}	β_1	β_2	Chord (mm)
76.2	0.27	71.87	40.77	84.3
101.6	0.36	72.81	43.50	81.5
127.0	0.45	76.56	46.30	78.8
152.4	0.55	78.37	49.94	75.9
177.8	0.64	79.52	52.13	73.1
203.2	0.73	80.31	53.64	70.6
228.6	0.82	82.87	56.51	68.1
254.0	0.91	84.00	58.39	65.8
279.4	1.00	85.21	60.92	63.8

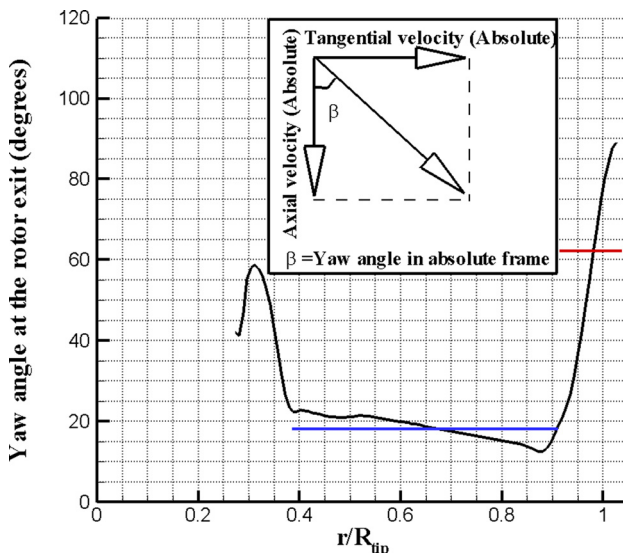


Fig. 3 Yaw angle in the absolute frame calculated from the initial computations

problem where the yaw angle varies dramatically near the tip section of the blade is extremely challenging. A computational fluid dynamics approach was used to properly align the probe with respect to the axial direction. Preliminary computations of the rotor exit flow field were performed using the Ansys CFX RANS solver. Details of this computational analysis can be found in the following sections. Figure 3 shows computed the distribution of the absolute flow yaw angle at the fan rotor exit where the Kiel probe was located. Figure 3 shows that the absolute yaw angle is not significantly changed near the mid-span for radial stations $0.38 \leq r/R_{\text{tip}} \leq 0.90$. The average yaw angle obtained on these stations is 18 deg, which is shown by the straight blue line in Fig. 3. The Kiel probe was aligned at this average angle at these locations. Although the flow angles varied by the effect of the three dimensional features such as the passage vortex and hub separation near the hub region, the Kiel probe was assumed to capture the flow field because of its ± 52 deg yaw angle tolerance. Because the tip region where $r/R_{\text{tip}} \geq 0.90$ was affected by the tip leakage vortex, the tangential velocity component changed due to this vortical field and the yaw angle abruptly increased in this region. The Kiel probe was manually aligned by the “averaged” computed absolute flow yaw angles in this region. The probe was aligned at 62 deg angle around the tip region.

The Kiel total pressure head was connected to a Validyne DP 15 variable reluctance pressure transducer that was referenced to atmospheric pressure. The output of the transducer was directly connected to the Validyne CD 15 carrier demodulator that gives a linearized analog output in the range of ± 10 V. The calibration of the pressure transducer required applying a known pressure to the transducer and recording the associated voltage. The relationship between the pressure and voltage was linear because an external demodulator linearization was employed. The Validyne carrier demodulator was connected to a 12-bit data acquisition board (MCC 1208FS). Analog signals were transferred to a computer and analyzed by Labview data acquisition software, which was custom developed for the current research effort. The 5 s data acquisition time was selected as the sampling time for the experiments so that the Kiel probe pneumatic output reached steady state and a statistically stable averaged total pressure reading was recorded.

The inlet conditions for the ducted fan system were also monitored using a Kiel total pressure probe and a conventional Pitot probe. Both probes were mounted over the duct lip at mid-span of the fan rotor. The conventional Pitot probe with a static and total hole measured the magnitude of the inlet axial velocity at mid-span. The total pressure at the duct inlet was measured using

the same procedure outlined for the rotor exit total pressure probe without “nulling.” The data acquisition time for this probe was also set to 5 s. A Pitot probe was used to obtain the duct inlet velocity. Both probes were aligned with the axial flow direction, since the flow at the inlet of the ducted fan is where the flow was free from tangential and radial components.

2.3.2 Six Component Force and Moment Measurement. The ducted fan aerodynamic research performed in this study requires high accuracy force and moment measurements. The 22 in. diameter fan is equipped with an ATI-Delta six component force and torque transducer. The ATI multi-axis force/torque sensor system measures all six components of the force and moment. Three components of force and three components of moments are measured. It consists of a transducer assembly, a shielded high-flex cable, and a 16-bit data acquisition system and an F/T controller. A software system provided by ATI was used to convert the transducer readings into force and torque output in engineering units using the calibration data provided. The thrust and moment transducer is factory calibrated with known forces and moments. The accuracy of the transducer was ± 0.033 N for forces in the x direction, ± 0.033 N for forces in the y direction, ± 0.099 N for forces in the z direction, ± 0.003 Nm for moments in the x direction, ± 0.003 Nm for moments in the y direction, and ± 0.003 Nm for moments in the z direction.

3 Computational Method

A three dimensional computational method is used for analyzing the viscous and turbulent flow fields around and inside the ducted fan and, especially, the complicated flow field near the fan rotor tip for the hover condition.

A simulation of the incompressible mean flow field around the ducted fan was performed using the general purpose fluid dynamics solver Ansys-CFX. The specific computational system solves the Reynolds-averaged Navier-Stokes (RANS) equations using an element based finite volume method in the ducted fan rotor and around the ducted fan driven VTOL UAV. The mass, momentum, and energy equations are simultaneously solved over an unstructured finite volume based mesh system.

The $k-\omega$ based shear stress transport model is used in our computations [20]. This model accounts for the transport of the turbulent shear stress and gives accurate predictions of the flow separation under an adverse pressure gradient.

3.1 Computational Domains and Boundary Conditions.

The computational analysis for the ducted fan aerodynamic investigation in hover was performed on three separate computational domains that are connected. The stationary inlet and outlet regions and rotating fan rotor region are shown in Fig. 5. The inlet region includes an inlet lip surface that was considered as a solid wall with the no-slip condition. Atmospheric static pressure was prescribed on the top surface. On the side surface, an opening type boundary condition was assumed. An opening boundary condition allows the fluid to cross the boundary surface in either direction. For example, all of the fluid might flow into the domain at the opening, or all of the fluid might flow out of the domain, or a combination of the two might occur. An opening boundary condition might be used where it is known that the fluid flows in both directions (any direction) across the boundary.

The outlet region includes the outer duct surface, circular rods, rotor hub surface, and the support structure underneath the system that is considered as solid walls with the no-slip condition. The bottom surface is also treated with the no-slip boundary condition. On the side surface, an opening boundary condition is assumed.

The rotating region includes fan blades, the rotor hub region, and the shroud surface where rotating fluid motion is simulated by adding source terms. Additional sources of momentum are required to account for the effects of the Coriolis force and the

PROOF COPY [TURBO-12-1212]

308 centrifugal force. Counter-rotating wall velocities are assigned at
309 the shroud surface.

310 Stationary and rotating regions were sub-sectional by periodic
311 surfaces. By using the periodicity, the speed of the numerical sim-
312 ulations was increased. The stationary surfaces were divided into
313 four segments and the rotating region was divided into eight peri-
314 odic segments. Only one of these segments for each region was
315 used in numerical calculations. The difference in the pitch angles
316 of the frames is taken into account in the ninterfaces that are
317 connecting the rotating and stationary surfaces. A stage type interface
318 model was used.

319 **3.2 Stage Interface.** When one side is in a stationary frame
320 and the other side is in a rotating frame of reference, an interface
321 should be used for connection. The “stage” type interface model
322 is used in calculations for modeling the frame change. The stage
323 model performs a circumferential averaging of the fluxes on the
324 interface. This model allows steady state predictions to be
325 obtained for turbomachinery components. The stage averaging at
326 the frame change interface introduces a one-time mixing loss.
327 This loss is equivalent to assuming the physical mixing supplied
328 by the relative motion between components. Between the station-
329 ary frames, an interface provides a general connection between
330 two stationary domains. The general grid interface is used for
331 mesh connections between interfaces.

332 **3.3 Grid Refinement Study.** A grid independence study is
333 performed to show that the computational results are not depend-
334 ent on the computational mesh and the resolution of the mesh is
335 adequate to capture the significant flow characteristics. The grid
336 independence is evaluated by comparing the computational solu-
337 tions from three different mesh sizes, comprising a coarse mesh
338 with 3,000,000 tetrahedral cells, a medium mesh with 4,750,000
339 cells, and a mesh with 6,000,000 cells. The static pressure distri-
340 bution around the mid-span blade profile at the radial station
341 $r = 0.90$ for the baseline fan rotor is plotted in Fig. 4 for three dif-
342 ferent grid densities. The profile suggests that the computational
343 results are grid independent when the 4,700,000 cells are
344 exceeded. Therefore, the medium mesh is used for all predictions
345 in this chapter. Figure 5 illustrates a view from the medium size
346 computational mesh near the inlet lip region and rotor tip. The
347 unstructured tetrahedral cells are used for the computations.
348 Regions near the solid surfaces are meshed with prisms for gener-
349 ating a better viscous boundary layer grid. A nondimensional wall

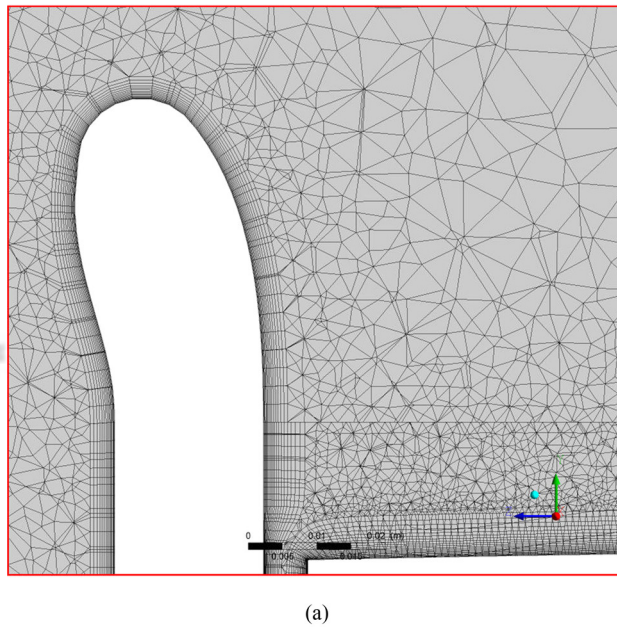
349 distance (y^+) of less than 2 is achieved near the shroud and hub
350 region. The region between the solid shroud and rotating blade
351 tips is filled with prism layers.

4 Experimental Results

352

4.1 Force and Torque Measurements. The most significant
353 force and moment component that is measured for the ducted fan
354 system in the hover condition is the thrust and rotor torque which
355 are F_z and T_z , as shown in Fig. 1. Other components may become
356 significant when the ducted fan is operated in nonsymmetric inlet
357 conditions, such as forward flight operation. Although three com-
358 ponents of forces and moments were measured, only the thrust
359 and torque of the ducted fan will be presented throughout this pa-
360 per since all of the measurements are performed in the hover con-
361 dition. The thrust and torque measurements were obtained at the
362 hover condition for a number of rotor speeds. Thrust measure-
363 ments are normalized as the thrust coefficient, defined as
364

$$C_T = \frac{\text{Thrust}}{\rho \Omega^2 D^4}, \quad \text{where} \quad \rho = \frac{P_a}{RT_a} \quad (1)$$



(a)

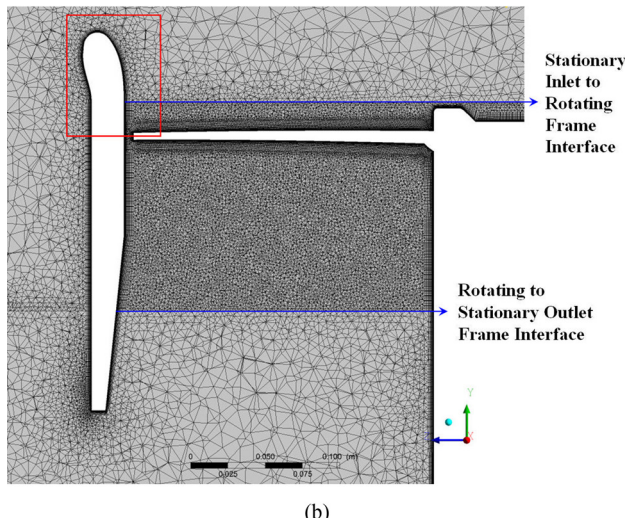


Fig. 5 Medium size computational mesh used in the computations

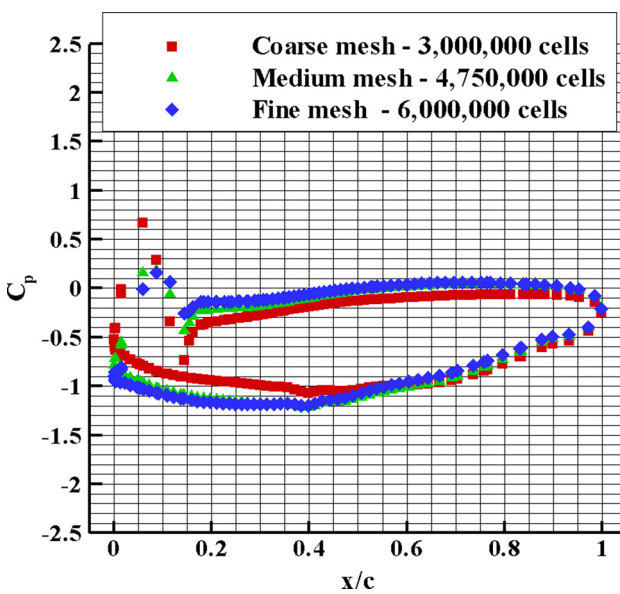


Fig. 4 Grid independence study

PROOF COPY [TURBO-12-1212]

365 Torque measurements were essential in calculating the
 366 required power using the relationship between torque and power
 367 (Power = Torque $\times \Omega$). The measured power was normalized as a
 368 power coefficient

$$C_P = \frac{\text{Power}}{\rho \Omega^3 D^5}, \quad \text{where} \quad \rho = \frac{P_a}{RT_a} \quad (2)$$

369 The figure of merit was calculated as a measure of hover effi-
 370 ciency for the ducted fan. The figure of merit was defined as

$$\text{Figure of merit: (FM)} = \frac{C_T^{3/2}}{\sqrt{2} C_P} \quad (3)$$

371 Figure 6 shows the calculated thrust coefficient for the 22 in.
 372 ducted fan with baseline fan rotors at various rotational speeds.
 373 The ducted fan thrust was measured for various tip clearances.
 374 The fan rotor only thrust was also measured. The fan rotor only
 375 thrust was measured by using the 10.89 in. tip diameter fan rotor,
 376 which is the identical rotor used for the 3.04% tip clearance study.
 377 The tip clearances were adjusted by changing the fan rotor diameter,
 378 as previously mentioned.

379 The variable tip clearance study presented in this chapter used
 380 custom made rotors with accurately adjusted tip diameters in a
 381 shroud system having a constant inner diameter. Using a ducted
 382 fan around an open rotor improves the thrust of the system as
 383 compared to an open rotor for tip clearances of 3.04% and 1.71%.
 384 For the tip clearance of 5.17%, the open rotor provides more
 385 thrust. This observation can be explained by the effect of
 386 increased viscous losses and tip leakage related losses. The losses
 387 generated when the shroud is added to the fan rotor is so high that
 388 the additional thrust due to the duct lip and shroud is almost eliminated.
 389 It should also be noted that decreasing the tip gap height is
 390 effective at improving the performance of the system and results
 391 in an augmented thrust generation.

392 The thrust force generated per supplied power for various base-
 393 line configurations is shown in Fig. 7. The data is arranged in the
 394 form of the thrust coefficient C_T versus the power coefficient C_P .
 395 The smallest tip clearance configuration generates the highest
 396 thrust per unit of power supplied. Since increasing the tip clear-
 397 ance also increases losses in the system, the power demand of the
 398 system also increases.

399 Figure 8 shows another key result of this study. The sensitivity
 400 of hover efficiency to increasing tip gap is shown. It should be
 401 noted that using a ducted fan configuration also improved hover

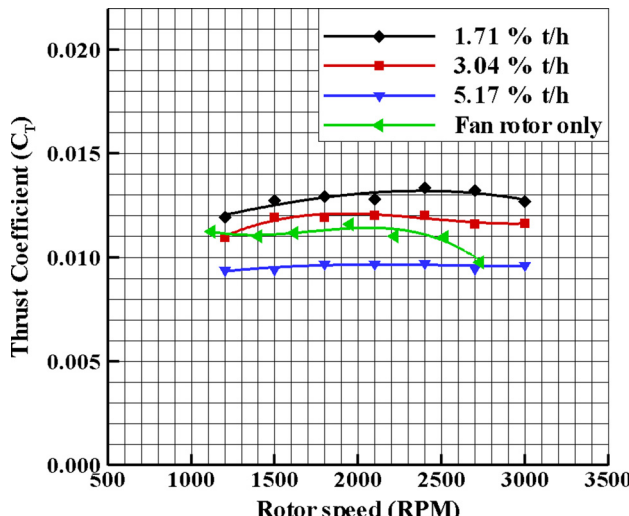


Fig. 6 Thrust coefficient versus the fan rotational speed during hover (baseline rotor)

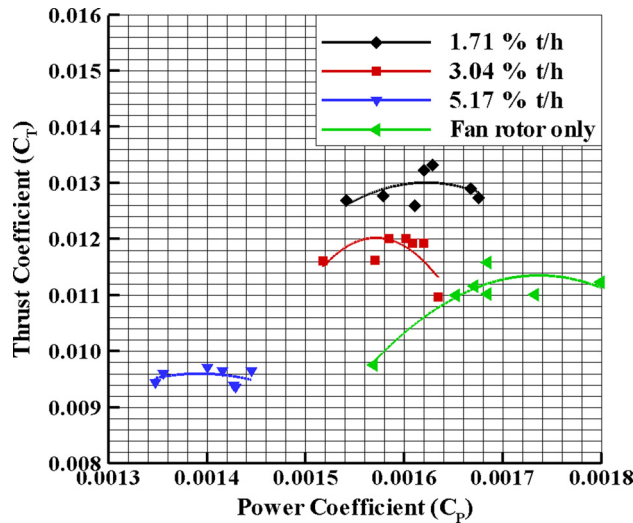


Fig. 7 Thrust coefficient versus the power coefficient for the baseline rotor

efficiency by 38% for the higher rotational speed. Decreasing the tip clearance is effective in increasing the hover efficiency. Decreasing the tip clearance from 3.04% to 1.71% increased the hover efficiency of the system by 17.85% at the higher rotor speed.

4.2 Total Pressure Measurements at Rotor Exit. The aerodynamic performance of the ducted fan was quantified by rotor exit total pressure measurements at the hover condition for 2400 rpm. The results are presented with the nondimensional total pressure coefficient, which is defined as

$$C_{pt} = \frac{P_{te} - P_{ti}}{\frac{1}{2} \rho U_m^2}, \quad \text{where} \quad \rho = \frac{P_a}{RT_a} \quad (4)$$

where U_m is the rotor speed calculated at the mid-span $U_m = r_m \times \Omega$. The random uncertainty of the total pressure coefficient was calculated as ± 0.002 [21,22].

Figure 9 shows the total pressure coefficient measured at the downstream position from the rotor hub to the shroud. It should

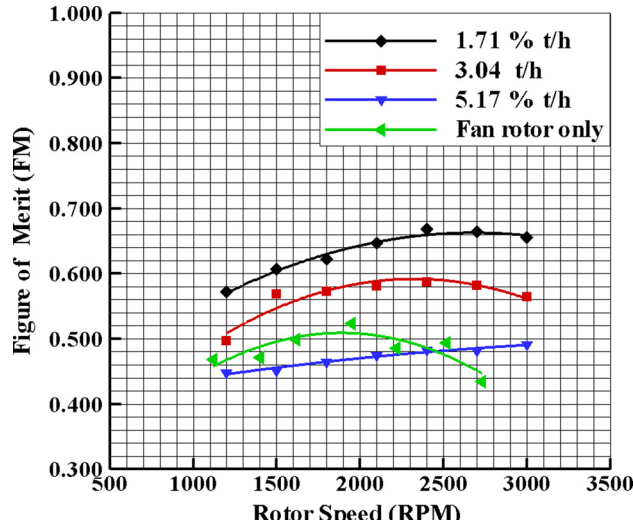


Fig. 8 Figure of merit (FM) versus the fan rotational speed for the baseline rotor

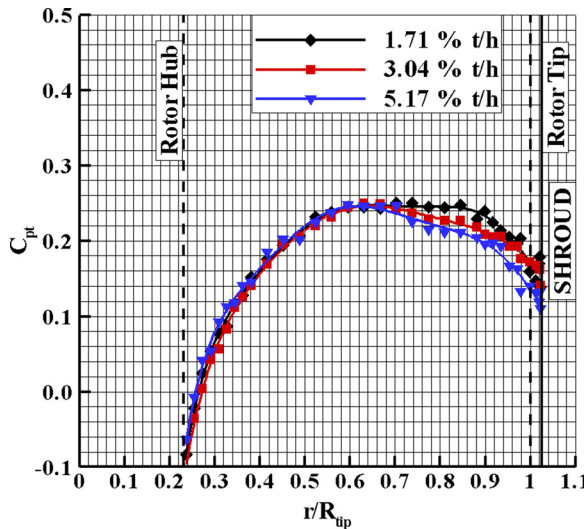
PROOF COPY [TURBO-12-1212]

Fig. 9 Total pressure measured downstream of the rotor at 2400 rpm for the baseline rotor

be noted that there is almost no change in the total pressure coefficient by changing the tip clearance for $r/R_{tip} \leq 0.65$. The flow near the rotor hub is not affected by the tip leakage losses. When the tip clearance is 5.17%, the losses related to the tip leakage vortex are increased at a significant rate because of the increased tip vortex size.

5 Computational Results

5.1 Computational Model Validation

5.1.1 Total Pressure at the Rotor Exit. Figure 10 shows a comparison of the experimental and computational results for 1.71%, 3.04%, and 5.17% tip clearances. The circumferentially averaged total pressure coefficient at the downstream of the fan rotor is compared to the experimental results. The computational and experimental results show very good agreement in the spanwise distribution, except in a limited area near the hub where $r/R_{tip} \leq 0.65$. The computational results slightly deviate from the experimental results near the hub region. That is because of the highly complex low Reynolds number and, possibly, re-circulatory turbulent flow field near the hub region. The low Reynolds number characteristic of the flow makes this computation highly challenging. The Reynolds number based on the blade chord is approximately lower than 50,000 at the $r/R_{tip} \leq 0.6$. Low Reynolds number flows are relatively hard to compute using standard turbulent models as they are used in present day computational systems. The overall results show significant re-circulatory flow zones near the hub wall. The highly 3D and possibly unsteady flow zones are driven by the hub inlet (corner) region flows.

5.1.2 Thrust and Power Curves. Figure 11 shows the variation of thrust with rotational speed obtained from experiments and the computational results for two different tip clearances. Clearly, the computational results agree well with the experimental data for both tip clearances, especially for low rotational speeds. The relative error increases for rotor speeds higher than 2400 rpm.

The computed rotor thrust and duct thrust are also shown in Fig. 11. As the tip clearance increases, the rotor thrust decreases because of the increased tip leakage flow. The tip leakage flow is quantified by calculating the leakage mass flow rate. The leakage mass flow rate is 1.81% of the mass flow rate of the fan rotor for the 1.71% tip clearance. When the tip clearance increased to 3.04%, the leakage mass flow rate is also increased to 3.41% of

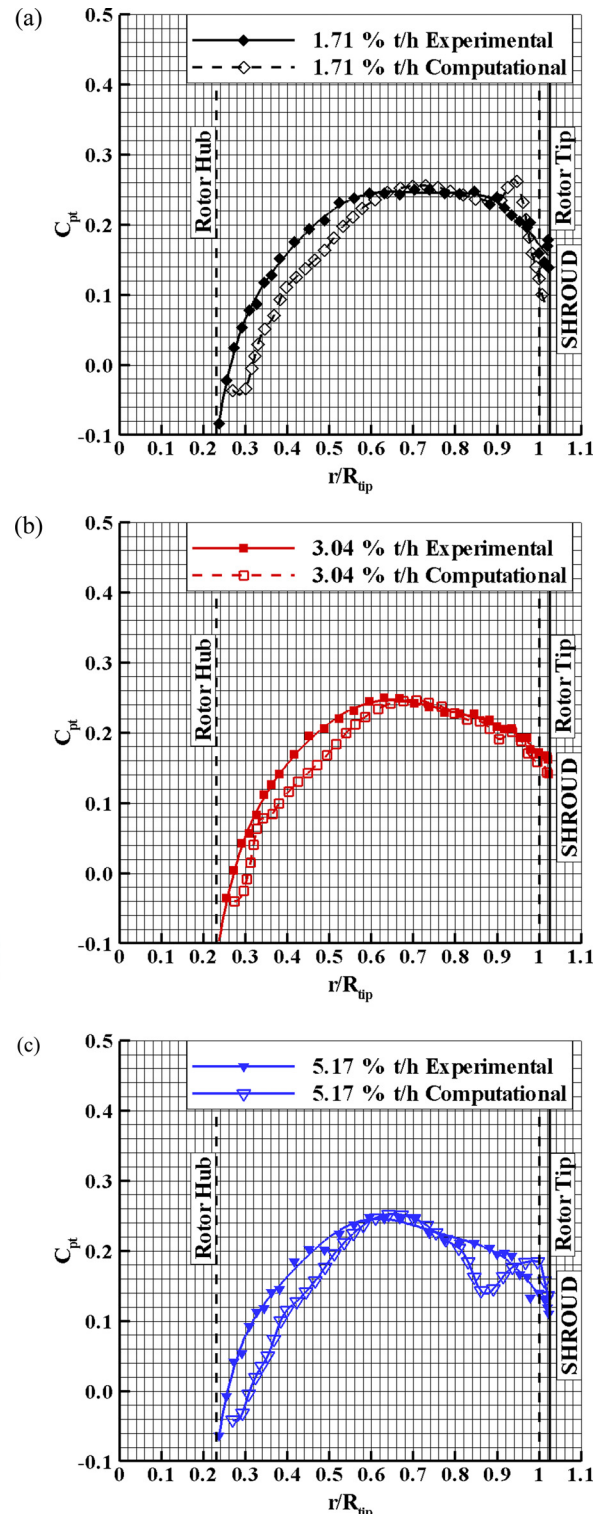


Fig. 10 Total pressure coefficient comparison for experimental and computational analysis at 2400 rpm for the baseline rotor with (a) 1.71%, (b) 3.04%, and (c) 5.17% tip clearances

the fan rotor mass flow rate. That increase in the leakage mass flow rate increased losses in the main fan flow and decreased rotor thrust. Although the duct thrust was the same for both tip clearances for low rotor speeds, it increased for a high rotor speed as the tip clearance decreased. The main reason for this improvement in duct thrust is an increase in the axial velocity component of the velocity, especially for high rotor speeds.

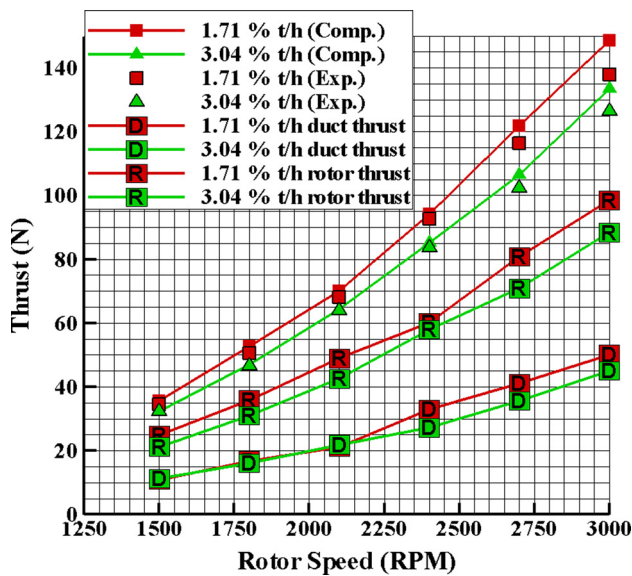
PROOF COPY [TURBO-12-1212]

Fig. 11 Comparison of the computed and measured thrust for 1.71% and 3.04% tip clearances for the baseline rotor

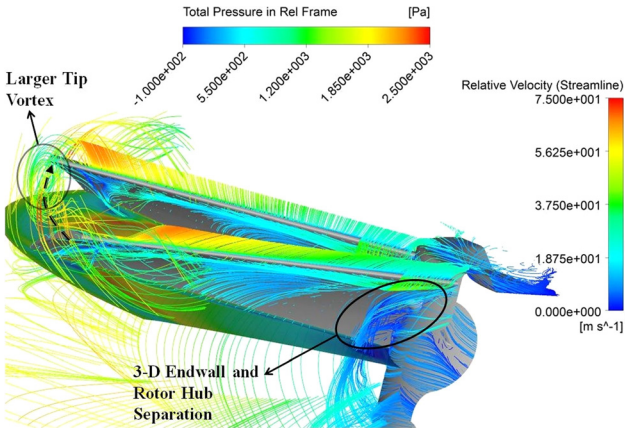


Fig. 12 Streamlines around the baseline rotor blade with a 1.71% tip clearance and the rotor hub at 2400 rpm

463 5.2 Flow Field Analysis

464 **5.2.1 Effect of Tip Leakage and Secondary Flows on Fan**
 465 **Rotor Exit Performance.** The flow field between the stationary
 466 shroud and rotor tip of a ducted fan is highly complex because of
 467 the interaction of the leakage flow, annulus wall boundary layer,
 468 and rotor wake. Figures 12 and 14 show the streamlines drawn
 469 around the rotor blade with the 1.71% and 3.04% tip clearance,
 470 respectively. The complex flow features near the tip and mid-span
 471 region are visualized at a high spatial resolution. Streamlines are
 472 colored by the relative velocity magnitude and drawn in the
 473 relative frame of reference. The leakage vortex impinges on the
 474 neighboring blade and creates a local loss region. This lossy
 475 region moves towards the mid-span as the clearance increased.
 476 The magnitude of the relative total pressure just at the down-
 477 stream of the fan rotor with 1.71% tip clearance is shown in
 478 Fig. 13. This figure is drawn just downstream of the fan rotor and
 479 the visualization plane is aligned with the trailing edge of the rotor
 480 blade. The red regions in the figure show the highest total pressure
 481 regions, while dark blue region show the lowest total pressure
 482 regions. The dark blue region near the fan rotor hub clearly shows
 483 the loss generation near the endwall surface due to the combina-
 484 tion of the hub corner separation and the three dimensional hub

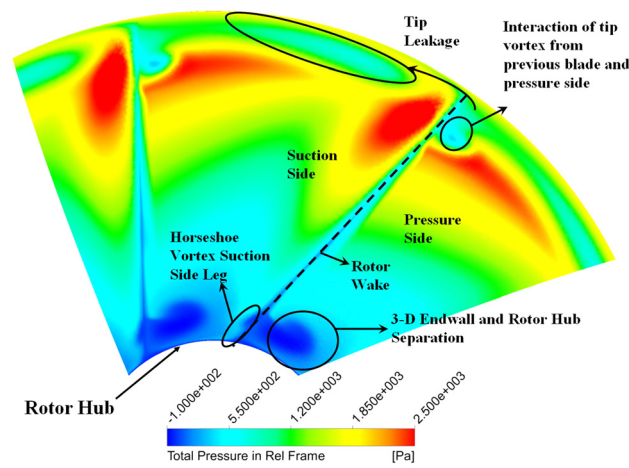


Fig. 13 Relative total pressure distribution at the rotor exit plane for the baseline blade with a 1.71% tip clearance

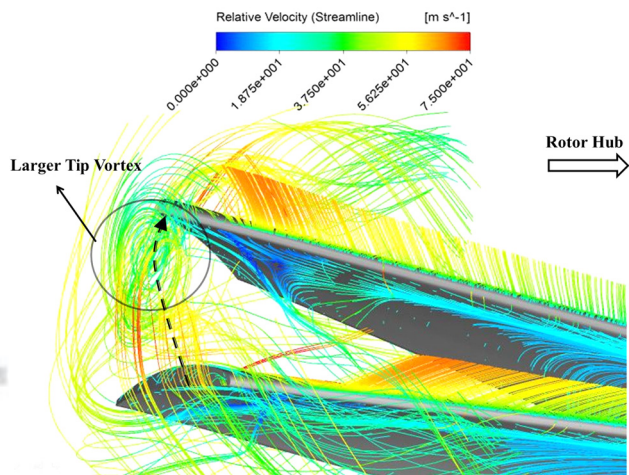


Fig. 14 Streamlines around the baseline rotor blade with a 3.04% tip clearance and the rotor hub at 2400 rpm

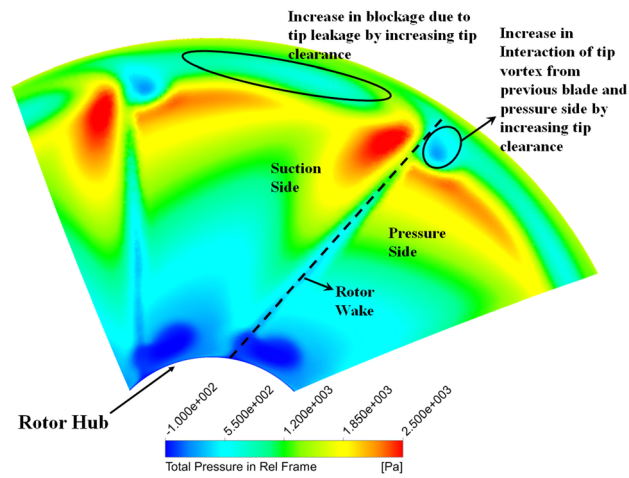


Fig. 15 Relative total pressure distribution at the rotor exit plane for the baseline blade with a 3.04% tip clearance

endwall flow. The wake region of the rotor blade is shown by dashed lines in Fig. 13. The tip leakage flow and tip vortex is also visible near the rotor tip. The light blue region near the rotor tip shows the blockage effect that is induced by the tip vortex

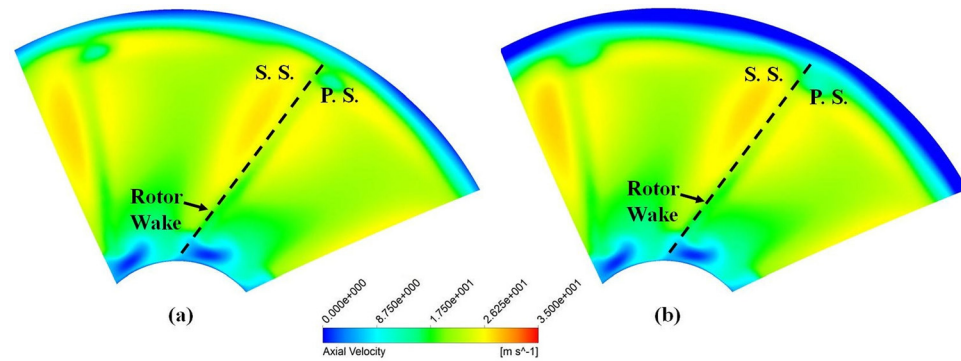


Fig. 16 Axial velocity comparison at the rotor exit plane for the baseline blade with (a) 1.71%, and (b) 3.04% tip clearances

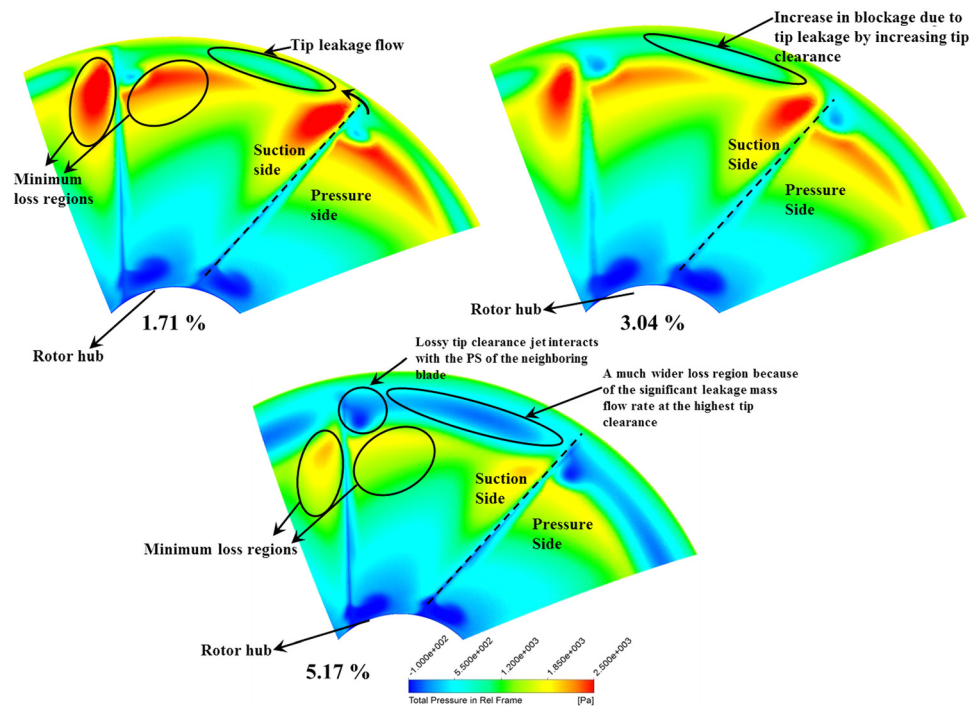


Fig. 17 Relative total pressure comparison at the rotor exit plane for the baseline blades with 1.71%, 3.04%, and 5.17% tip clearances

489 originating from the rotor blade pressure side. There is also
 490 another light blue region near the pressure side of the rotor blade.
 491 That shows the interaction of the tip vortex propagating from the
 492 previous rotor blade with the pressure side, as shown in Fig. 13.
 493 This interaction can also be seen in Fig. 12 by the streamlines
 494 drawn around the rotor tip. This interaction near the pressure side
 495 results in a measurable total pressure drop at the exit of the fan
 496 blade because of separation from the pressure side.

497 Figure 15 shows the effect of the tip clearance and other important
 498 3D passage flow features on the rotor exit relative total pressure
 499 distribution for a tip clearance value of 3.04%. This figure is
 500 drawn at the same plane that is used in Fig. 13. Changing the
 501 clearance level did not affect this distribution near the hub region.
 502 However, an increase in the tip clearance resulted in more
 503 aerodynamic loss near the rotor tip. The overall blockage due to
 504 tip leakage is also increased. Besides, the interaction of the tip
 505 vortex and rotor blade pressure side is greatly enhanced and more
 506 total pressure loss is obviously generated in the passage. Figure 16
 507 shows the comparison of the axial velocity at the downstream of
 508 the fan rotor. The low momentum fluid near the hub region is

509 shown by a dark blue color. This region was not affected by
 510 changing the tip clearance level. The tip leakage losses were
 511 increased by increasing the tip clearance. An increase in the size
 512 of the blockage due to the tip vortex is observed by comparing the
 513 dark blue regions near the casing for 1.71% and 3.04% tip
 514 clearances. The size of the dark blue area increased for the 3.04% tip
 515 clearance.

516 The effect of increasing the tip clearance is shown in Fig. 17.
 517 Three different tip clearances were compared by total pressure
 518 contours drawn at the downstream of the fan rotor and the visual-
 519 ization plane is aligned with the trailing edge of the rotor blade.
 520 When the tip clearance was increased to 5.17%, tip leakage losses
 521 were tremendously increased due to a stronger tip clearance jet.
 522 This lossy leakage flow interacts with the pressure side of the
 523 neighboring blade. This impinging leakage jet creates a relatively
 524 large local loss region and moves towards the mid span. A
 525 much wider total pressure loss region was created because of the
 526 significant leakage mass flow rate at the highest tip clearance. The
 527 minimum loss regions indicated by red are shrinking, as shown by
 528 the orange and yellow zones for the 5.17%.

529 6 Conclusions

530 Experimental investigations and computational analyses were
 531 performed for the development of novel tip geometries that are
 532 applicable to ducted fans used in VTOL UAV systems. The com-
 533 putational method that will be a major design analysis tool for the
 534 design of novel tip geometries is validated via experimental data
 535 presented throughout this paper.

536 A 22 in. diameter ducted fan test system was designed and
 537 manufactured for experimental investigations of tip leakage flow
 538 in ducted fans. Fan rotor exit total pressure surveys and duct inlet
 539 total pressure and velocity measurements were carried out for
 540 aerodynamic performance quantifications. A six component force
 541 and torque transducer was used for aeromechanical performance
 542 quantification.

543 A high resolution simulation of the flow field around the rotat-
 544 ing fan rotor blades was performed by solving Reynolds-averaged
 545 Navier-Stokes equations using a general purpose solver, Ansys-
 546 CFX. The computational analysis was extensively used in designing
 547 the tip treatments.

548 When the 3.04% clearance results are compared to the rotor
 549 only result, up to a 38% increase in ducted fan hover efficiency
 550 can be obtained at higher rotor speeds. That increase is mainly the
 551 result of using a duct around an open rotor.

552 A steady-state RANS simulation of fan rotor blades and duct
 553 geometry showed very good agreement with the measured total
 554 pressure distribution, especially near the tip region of the rotor in
 555 the 22 in. diameter ducted fan research facility.

556 Experimental investigations of the baseline rotor showed that
 557 decreasing the tip clearance increased the thrust obtained from the
 558 ducted fan in the hover condition. Decreasing the tip clearance
 559 from 3.04% to 1.71% also increased the hover efficiency of the
 560 system by 17.85% at higher rotor speeds.

561 When the tip clearance increased from 3.04% to 5.17%, up to
 562 an 18.1% drop in hover efficiency was observed.

563 Since the agreement between the experimental results obtained
 564 from the 22 in. diameter ducted fan and the 3D RANS based com-
 565 putations is very good, the present computational tool forms a
 566 strong design/analysis basis for future tip treatments that can be
 567 developed by computational means.

568 The results from an investigation dealing with the new tip treat-
 569 ments designed and analyzed using this validated computational
 570 approach are presented in an accompanying paper by Akturk and
 571 Camci [18].

572 Acknowledgment

573 The authors acknowledge the financial support provided by the
 574 PSU Vertical Lift Center of Excellence (VLRCOE) and the
 575 National Rotorcraft Technology Center (NRTC) (Under U.S.
 576 Army Research Office Grant No. W911W6-06-2-0008). They
 577 wish to thank Ozhan Turgut for his support throughout this effort.
 578 They are also indebted to Mr. Harry Houtz for his technical
 579 support.

580 Nomenclature

581 c	= chord length	
C_p	= static pressure coefficient	
C_{pt}	= total pressure coefficient, $C_{pt} = P_{te} - P_{ti}/(1/2)\rho U_m^2$	
C_P	= power coefficient, $C_P = \text{Power}/\rho\omega^3 D^5$	
C_T	= thrust coefficient, $C_T = \text{Thrust}/\rho\omega^2 D^4$	
D	= shroud (casing) inner diameter (m)	
582 h	= blade height	

IC	= internal combustion	583
p	= static pressure	584
PS	= pressure side	585
R	= ideal gas constant (for air $R = 287 \text{ J/Kg K}$)	
RANS	= Reynolds-averaged Navier-Stokes	
SS	= suction side	586
t	= effective tip clearance in inches	587
t/h	= relative tip clearance with respect to blade height	588
UAV	= uninhabited aerial vehicles	
VTOL	= vertical take-off and landing	
y^+	= nondimensional wall distance	

References

- [1] Lee, G. H., Baek, J. H., and Myung, H. J., 2003, "Structure of Tip Leakage in a Forward Swept Axial-Flow Fan," *Flow, Turbul. Combust.*, **70**, pp. 241–265.
- [2] Jang, C. M., Furukawa, M., and Inoue, M., 2001, "Analysis of Vortical Flow Field in a Propeller Fan by LDV Measurements and LES—Part I, ii," *ASME J. Fluids Eng.*, **123**, pp. ■.
- [3] Jang, C. M., Furukawa, M., and Inoue, M., 2001, "Analysis of Vortical Flow Field in a Propeller Fan by LDV Measurements and LES—Part I," *ASME J. Fluids Eng.*, **123**, pp. ■.
- [4] Storer, J. A. and Cumpsty, N. A., 1991, "Tip Leakage Flow in Axial Compressors," *ASME J. Turbomach.*, **113**, pp. ■.
- [5] Lakshminarayana, B., Zaccaria, M., and Marathe, B., 1995, "The Structure of Tip Clearance Flow in Axial Flow Compressors," *ASME J. Turbomach.*, **117**, pp. 336–347.
- [6] Matzgeller, R., Bur, P., and Kawall, J., 2010, "Investigation of Compressor Tip Clearance Flow Structure," *Proceedings of the ASME Turbo Expo 2010: Power for Land, Sea and Air*, Paper No. GT2010-23244.
- [7] Inoue, M., Kuromaru, M., and Furukawa, M., 1986, "Behavior of Tip Leakage Flow Behind an Axial Compressor Rotor," *ASME J. Gas Turbines Power*, **108**, pp. 7–14.
- [8] Furukawa, M., Inoue, M., Kuromaru, M., Saik, I. K., and Yamada, K., 1999, "The Role of Tip Leakage Vortex Breakdown in Compressor Rotor Aerodynamics," *ASME J. Turbomach.*, **121**, pp. 469–480.
- [9] Fujita, H. and Takata, H., 1984, "A Study on Configurations of Casing Treatment for Axial Flow Compressors," *Bull. JSME*, **27**, pp. 1675–1681.
- [10] Moore, R. D., Kovich, G., and Blade, R. J., 1971, "Effect of Casing Treatment on Overall and Blade-Element Performance of a Compressor Rotor," NASA Technical Report No. TN-D6538.
- [11] Reynolds, B., Lakshminarayana, B., and Ravindranath, A., 1979, "Characteristics of Near Wake of a Fan Rotor Blade," *AIAA J.*, **17**, pp. 959–967.
- [12] Ravindranath, A. and Lakshminarayana, B., 1980, "Mean Velocity and Decay Characteristics of Near and Far-Wake of a Compressor Rotor Blade of Moderate Loading," *ASME J. Eng. Power*, **102**, pp. 535–547.
- [13] Myung, H. J. and Baek, J. H., 1999, "Mean Velocity Characteristics Behind a Forward Swept Axial-Flow Fan," *JSME Int. J.*, **42**, pp. 476–488.
- [14] Williams, R., Ingram, G., and Gregory-Smith, D., 2010, "Large Tip Clearance Flows in Two Compressor Cascades," *Proceedings of the ASME Turbo Expo 2010: Power for Land, Sea and Air*, Paper No. GT2010-22952.
- [15] Pereira, J. L., 2008, "Hover and Wind-Tunnel Testing of Shrouded Rotors for Improved Micro Air Vehicle Design," Ph.D. thesis, University of Maryland, College Park.
- [16] Martin, P. and Tung, C., 2004, "Performance and Flowfield Measurements on a 10-Inch Ducted Rotor VTOL UAV," *60th Annual Forum of the American Helicopter Society*.
- [17] Martin, P. B., and Boxwell, D. A., 2005, "Design, Analysis and Experiments on a 10-Inch Ducted Rotor VTOL UAV," *AHS International Specialists Meeting on Unmanned Rotorcraft: Design, Control and Testing*.
- [18] Akturk, A., and Camci, C., 2011, "Tip Clearance Investigation of a Ducted Fan Used in VTOL UAVS—Part 1: Novel Treatments via Computational Design and Their Experimental Verification," *Proceedings of the ASME Turbo Expo 2011: Power for Land, Sea and Air*, Paper No. GT2011-46359.
- [19] United Sensors Corp., U.S., "United Sensors Corporation Kiel Probe: General Information," <http://www.unitedsensorcorp.com/kiel.html>
- [20] Wilcox, D. C., 1993, *Turbulence Modeling for CFD*, La Caada: DCW Industries, Canada.
- [21] Abemethy, R. B., Benedict, R. P., and ■, B., ■, D. R., 1985, "ASME Measurement Uncertainty," *ASME J. Fluids Eng.*, ■, pp. ■.
- [22] Abemethy, R. B., and ■, B., R., 1985, "The History and Statistical Development of the New ASME-SAE-AIAA-ISO Measurement Uncertainty Methodology," *AIAA/SAE/ASME/ASEE 21st Joint Propulsion Conference and Exhibit*.